iJRASET
International Journal For Research in Applied Science and Engineering Technology

INTERNATIONAL JOURNAL FOR RESEARCH

IN APPLIED SCIENCE & ENGINEERING TECHNOLOGY

Volume: 9 **Issue:** VI **Month of publication:** June 2021

DOI: https://doi.org/10.22214/ijraset.2021.35477

www.ijraset.com

Call: 08813907089 | E-mail ID: ijraset@gmail.com

International Journal for Research in Applied Science & Engineering Technology (IJRASET)
ISSN: 2321-9653; IC Value: 45.98; SJ Impact Factor: 7.429
Volume 9 Issue VI Jun 2021- Available at www.ijraset.com

High Cycle Fatigue Appearance of 10wt% cr steel and Dissimilar Metal Weld

Er. Hilal Ahmad Shah[1], Er. Puneet Bansal[2]
[1]*Student, Master of Technology,* [2]*Assistant Professor, Mechanical Engineering, Desh Bhagat University, Mandi Gobindgarh Punjab*

Abstract: ***The present study deals with the high cycle fatigue (HCF) behavior of a ten wt% Cr steel at ambient also as high temperatures (300–853 K). S–N curves were created at unlike temperatures using an R-ratio of −1. Outcome of mean stress was established over and done with Haigh diagram at 853 K using different R-values. Fatigue life was found to decrease with upsurge in test temperature and stress amplitude. Fatigue life was attempted using Basquin equation. Detailed fracture surface analysis was performed to study the crack initiation and propagation modes towards empathetic the mechanisms of failure at different temperatures.***

I. INTRODUCTION

10 wt% Cr steel belongs to series of 9-12 wt% ferritic steels, with a typical microstructure comprising of martensitic laths decorated with Cr-rich precipitates. Compared to austenitic steels, 10 wt% Cr steel features a higher strength, lower coef ficient of thermal expansion and a better thermal conductivity. thanks to martensitic structure and therefore the balance in chemical composition, the steel possesses an honest ductility and toughness, together with adequate heat strength. The steel is meant to be used within the low-pressure turbine section of the indigenous advanced ultra-supercritical power plants (AUSC-PP) which are expected to miti gate the CO_2 emissions and thereby help preserve the coal deposits in India for extended usage [1-5]. Components of low-pressure turbines within the AUSC-PP are subjected to severe flow-induced vibrations and thermal pressure fluctuations resulting in considerable HCF damage. This necessitates an in depth study on the HCF behavior of 10 wt% Cr steel. this investigation is predicated on the HCF behavior of 10 wt% Cr steel over a good range of temperature (300-853 K) and establishes important constant life diagrams that are necessary for the planning of those components against HCF.

A. Zeal for the Present Work

In order to moderate the CO2 emissions and preserve the coal deposits in India for longer usage, A-USC power plant technologies are being developed in the country which includes the design of the various components of the plant. The rotor of the proposed A-USC power plant consists of 3 distinct zones based on temperature and pressure conditions.

(a) High pressure turbine (HPT).
(b) Intermediate pressure turbine (IPT).
(c) Low pressure turbine (LPT).

To decrease the overall cost, the components of Low pressure turbine (LPT) have been chosen as 10wt% Cr steel. DMW joint between 617M & 10wt% Cr steel will also be used in the components of the turbine.

B. Objectives of this Study

1) To look at the influence of temperature on the fatigue life at a wide range of temperature (300 K- 853 K), R = -1 for 10wt%Cr steel.
2) To examine the combined influence of mean stress (σ_m) and stress amplitude (σ_a) on the cyclic life under HCF at 853 K for 10wt%Cr.
3) To calculate fatigue parameters using Basquin equation for 10wt%Cr ferritic steel.
4) To compare, by using evaluated fatigue parameters, expected and experimental life of 10wt%Cr.
5) To investigate the influence of stress amplitude unlike metal weld on at 853 K, R = -1.
6) To c alculate the micro-hardness of tested and untested unlike metal weld.

ISSN: 2321-9653; IC Value: 45.98; SJ Impact Factor: 7.429
Volume 9 Issue VI Jun 2021- Available at www.ijraset.com

II. LITERATURE REVIEW

A. Background

A-USC power plants are meant to operate at high pressures beyond the critical point (beyond 226 kg/cm2). Design of super-heater, re-heater, rotor materials and equipment development constitute significant areas to be addressed in this situation. The main components whose presentation is critical for A-USC power plants are high pressure steam piping and headers, super-heater tubing, water wall tubing and rotor. All of them have to meet the stipulated creep and fatigue strength requirements. In addition pipes, headers and rotor being heavy section components, are subject to fatigue induced by thermal stresses and vibrations. The materials for such applications should have adequate high temperature mechanical strength, high thermal conductivity and low coefficient of thermal expansion to minimize thermal stresses along with good formability. 10wt%Cr Steel is the candidate material for the rotor of the LPT and DMW weld joint for the overall design of the rotor of the turbine respectively.

B. Fatigue Examination

Fatigue is the failure of a material as a result of repeated number of cyclic loads that are even
Below the ultimate tensile stress limit, or the yield stress limit. It is the progressive and localized Structural damage and the most predominant failure mode in service and it is estimated that 90% of service failure of metallic components are caused by fatigue. Fatigue is usually associated with tensile stresses but fatigue cracks have been reported due to compressive loads as well [8]. Fatigue is typically conceptualized as a three-stage process consisting of initiation, propagation and subsequent premature failure. The duration of each of these three phases depends on many factors including the material and its processing history, the magnitude and direction of the applied stresses, the environment and the Temperature. Fatigue failures are typically characterized as either low cycle (Nf < 104 cycles)
Or high cycle (Nf > 104 cycles) Where Nf is the number of cycles to failure. The basic method of representing the fatigue data is S-N curve, which is a plot of stress vs number of cycles to Failure (Nf). The stress values are generally nominal values. Certain materials, primarily BCC Materials have an endurance limit or fatigue limit, which is a stress level below which material Has an “infinite” life (usually 1 million cycles). The endurance limit is due to interstitial Elements, such as carbon or nitrogen in iron, which pin dislocations. This prevents the slip Mechanism which leads to micro-cracks formation. Most nonferrous alloys have no endurance Limit and S-N line has a continuous slope as shown in Fig. 2.1. In the present context high cycle Fatigue behavior on 10wt%Cr Steel and DMW is discussed.

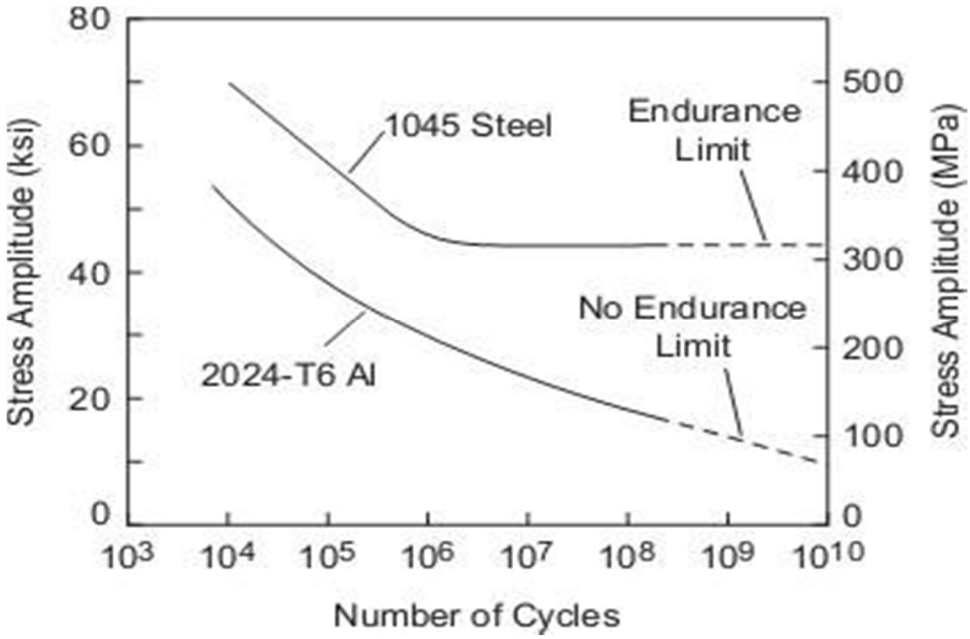

Fig. 2.1: S-N diagram of different materials [9].

1) Effect of Mean Stress on HCF

The mean level of the imposed cycle is known to play an important role on the HCF behaviour of engineering materials. An increase in σ_m (for a fixed value of σ_a) will always cause a reduction in the fatigue life [17, 18] (Fig. 2.2 (a)). The two most commonly used methods for depicting S-N data when σ_m is not equal to zero are as follows [18].

a) σ_{max} is plotted against log N for constant values of stress ratio (*R*). This is achieved by applying a series of stress cycles with decreasing σ_{max} and adjusting σ_{min} so as to maintain a constant value of R (Fig.2.2 (a)).

b) σ_a is plotted against cycles to failure at constant values of σ_m (Fig.2.2 (b)).

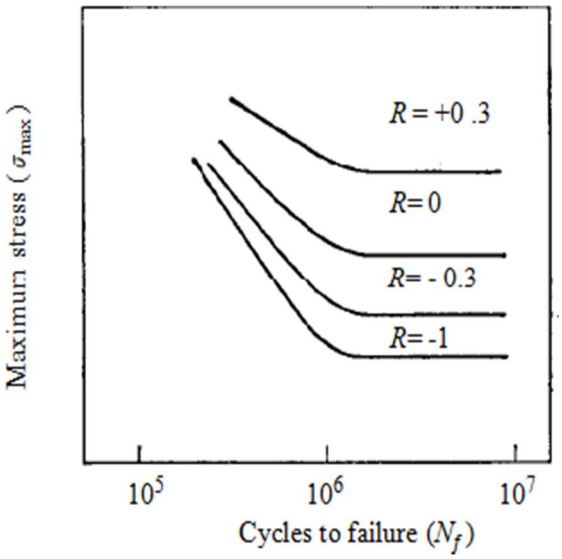

Fig.2.2(a):Method of plotting fatigue data [17]

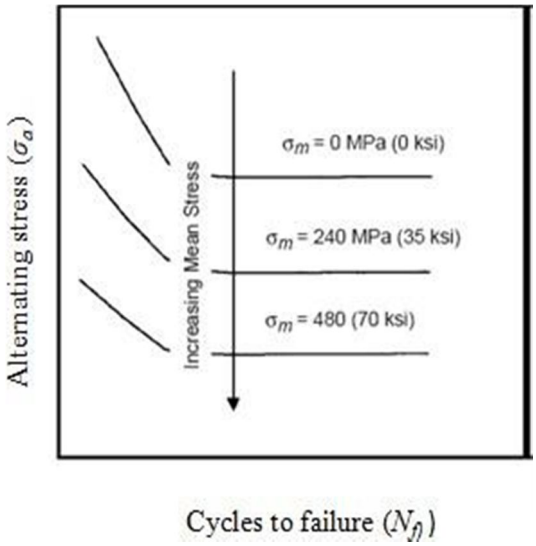

Fig.2.2(b):Method of plotting fatigue data[18]

A number of mathematical models have been developed that allow the effects of mean stress and stress amplitude to be predicted from fully reversed bending data. Goodman [19] developed a linear model (Eq. 2.2), while Gerber [20] (Eq.2.3) used a parabolic model (Fig.2.3). Test data for ductile metals usually fall closer to the Gerber parabolic curve; however, because of the scatter in fatigue data and the fact that notched data fall closer to the Goodman line, the more conservative Goodman relationship is often used in practice. If the component design is based on yield rather than ultimate tensile strength, as is more common, then the even more conservative Soderberg relationship (Eq.2.4) can be used.

$$\sigma_a = \sigma_e [1 - (\frac{\sigma_m}{\sigma_u})^x] \quad \text{.....Eq.2.1}$$

$$\sigma_a = \sigma_e [1 - \frac{\sigma_m}{\sigma_u}] \quad \text{.....Eq.2.2}$$

$$\sigma_a = \sigma_e [1 - (\frac{\sigma_m}{\sigma_u})^2] \quad \text{.....Eq.2.3}$$

$$\sigma_a = \sigma_e [1 - \frac{\sigma_m}{\sigma_y}] \quad \text{.....Eq.2.4}$$

Where, x=1 for the Goodman line, x=2 for the Gerber curve, $\sigma_u=\sigma_y$ for the Soderberg curve, and σ_e is the fatigue limit for completely reversed bending, σ_a= Fatigue strength for *N* cycles under mean stress of σ_m, σ_u= Ultimate tensile strength, σ_y= Yield strength.

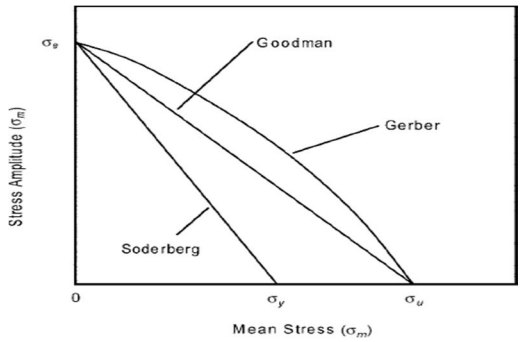

Fig. 2.3: Comparison of Goodman, Gerber and Soderberg models for relating mean stress to stress amplitude [18].

The Haigh diagram is another way of representing the fatigue data. It is a plot of alternating stress vs mean stress indicating the allowable stress for different constant lives (10^4,10^5,10^6,10^7), in contrast to single constant life shown in Goodman and Soderberg models.

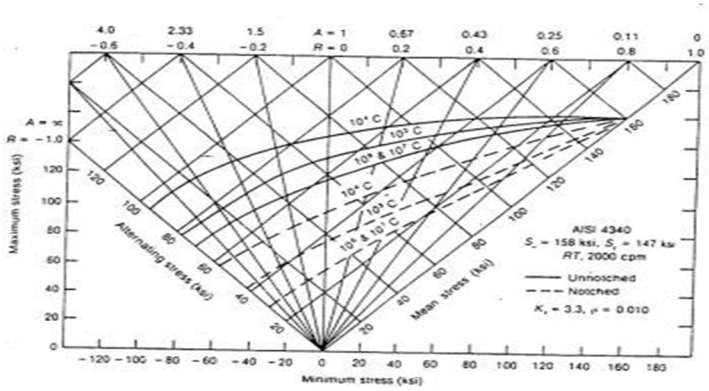

Fig. 2.4: Master diagram of steel AISI4340 (Haigh diagram) [18].

In Fig. 2.4, the combined effect of mean stress and alternating stress is presented with the aid of maximum and minimum stresses. It may be noted that as the *R* becomes more positive (which implies an increase in the mean stress) for a constant maximum stress, the fatigue life increases. On the other hand, for a constant alternating stress, as the *R* becomes more positive, the fatigue life decreases.

2) *High Cycle Fatigue (HCF):* HCF involves a large number of cycles (N f > 10 5 cycles) and an applied stress in the elastic regime [10]. HCF tests are typically carried out for 107 cycles and sometimes 5 x 10 8 cycles for nonferrous metals. Although the global stress is low enough to be elastic, plastic deformation could take place in localized regions such as surface discontinuities, scratches, machine marks etc., due to local stress concentrations, leading to initiation of cracks. HCF is usually presented as a plot of alternating stress versus the number of cycles to failure, Nf
3) *Effect of Temperature:* Generally lowering temperature will cause a slight rise in fatigue strength and vice versa. Fall in fatigue strength is progressively greater the nearer the temperature approaches melting point of the material. As the temperature rises, the mode of fracture tends to change to inter- crystalline, because grain boundary fracture tends to become easier than trans-crystalline slip. Different materials will react in slightly different ways under similar conditions, but any phase changes in a material will cause a marked divergence from the normal behavior. Also due to internal heating that occur in a material during cyclic loading may cause acceleration of a phase or structure change and may therefore influence both fatigue and creep strength. The effect is likely to weakening, but if change leads to a stiffening of the material lattice, a strengthening may occur. Other effect of temperature is thermal fatigue which is fatigue failure as the result of stresses setup by dimensional change during thermal cycling of a component. Its importance depends very much on circumstances and is influenced both by the shape of the component and the mode of thermal change

4) *Effect of DSA on fatigue behavior of alloy 617:* Generally fatigue failures often result from the applied stress levels that are below the yield point of the corresponding material. Sarkar et al. [68] studied the effect of DSA on HCF properties of this alloy and they showed that the fatigue life increases with decrease in stress amplitude which is lower than the YS, finally leading to run-out (knee point). But at 923 K, run-out was observed at stresses that were above the YS, contrary to the finite fatigue lives at stresses below the YS at ambient temperature as shown in Fig.2.14.

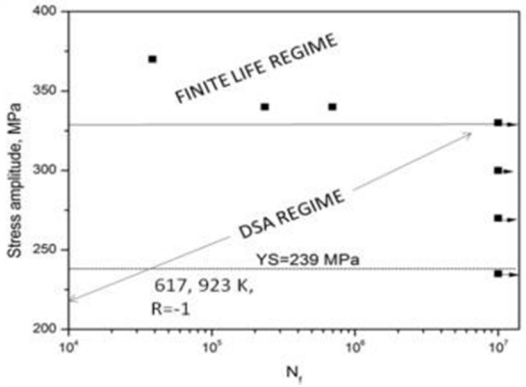

Fig. 2.13: Stress life plot for alloy 617M at 923 K [68].

Cabet et al. [73] studied the cyclic life and creep-fatigue life behavior of alloy 617 at 1223K with different strain rates. The result shows that in low cycle fatigue behaviour, at lower % of total strain the cyclic life is high and vice versa. The continuous cycle specimens exhibited trans-granular cracking and whenever the hold time is introduced specimens exhibited inter- granular cracking. The transition from trans-granular to inter-granular cracking is partially due to the environment.

Maier et al. [74] compared the fatigue lives of solution-annealed (1448 K/ 1 h/ water) and aged (1448 K/ 1 h/ water + 1253K/ 3 h/ air + 973 K/ 1 yr/ air). Conditions of Nickel based super-alloy 617B in low cycle fatigue condition. At the room temperature annealed specimens exhibited lowest peak stress than aged specimens, but at high temperature reverse behavior is exhibited. At high temperatures hardening rate of annealed material is high compared to aged material. However the decrease in peak stress aged specimens is due to continuous necking of specimens as a consequence of difficulties in strain control due to severe DSA at high temperatures.

III. EXPERIMENTAL DETAILS

A. *Introduction*

This chapter discusses the chemical composition of the material considered for the present study, specimen geometries, experimental procedures adopted for fatigue testing, test matrix and specimen characterization.

B. *Material Composition*

The chemical composition of forged products of 10wt%Cr Steel and DMW is given in Tables 3.1, 3.2. Specimen blanks were extracted from the forging.

Table 3.1: Chemical composition of 10wt%Cr Steel.

Element	C	Si	Mn	P	S	N	Al
Wt%	0.11-0.14	0.12 max	0.40-0.50	0.013 max	0.005 max	0.045-0.060	$\leq$0.010
Element	Cr	Mo	Nb	Ni	V	W	
Wt%	10.2-10.6	1.0-1.11	0.04-0.06	0.70-0.80	0.15-0.25	0.95-1.06	

Table 3.2: Chemical composition of DMW.

Base metal/10wt%Cr Steel									
Element	C	Si	Mn	P	S	N	Al	Cr	Mo
Wt%	0.11-0.14	0.12 max	0.40-0.50	0.013 max	0.005 max	0.045-0.060	≤0.010	10.2-10.6	1.0-1.11
Element	Nb	Ni	V	W					
Wt%	0.04-0.06	0.70-0.80	0.15-0.25	0.95-1.06					
Base metal /617M									
Element	C	Mo	Fe	Co	Ti	Cr	Si	Al	Ni
Wt. %	0.07	9.1	0.12	11.6	0.4	22.3	0.02	1.2	Bal
Butter layer									
Element	C	Si	Mn	P	S	Co	Al	Cr	Mo
Wt%	0.1	0.32	0.43	0.008	0.003	11.3	11.30	22.4	8.7
Element	Ti	Ni	Cu	Fe					
Wt%	0.43	Bal	0.10	0.80					

C. Sample Fabrication

10wt%Cr Steel was obtained from the cylindrical forging of diameter 200 mm. To get maximum number of specimens, blanks of diameter 16.5 mm were cut as per the scheme shown in Fig. 3.1. The HCF samples with threaded ends were machined through wire-cut EDM process. Surface finish operations were done through hand grinding process. In the similar manner the samples were obtained from the hollow forged tube for DMW.

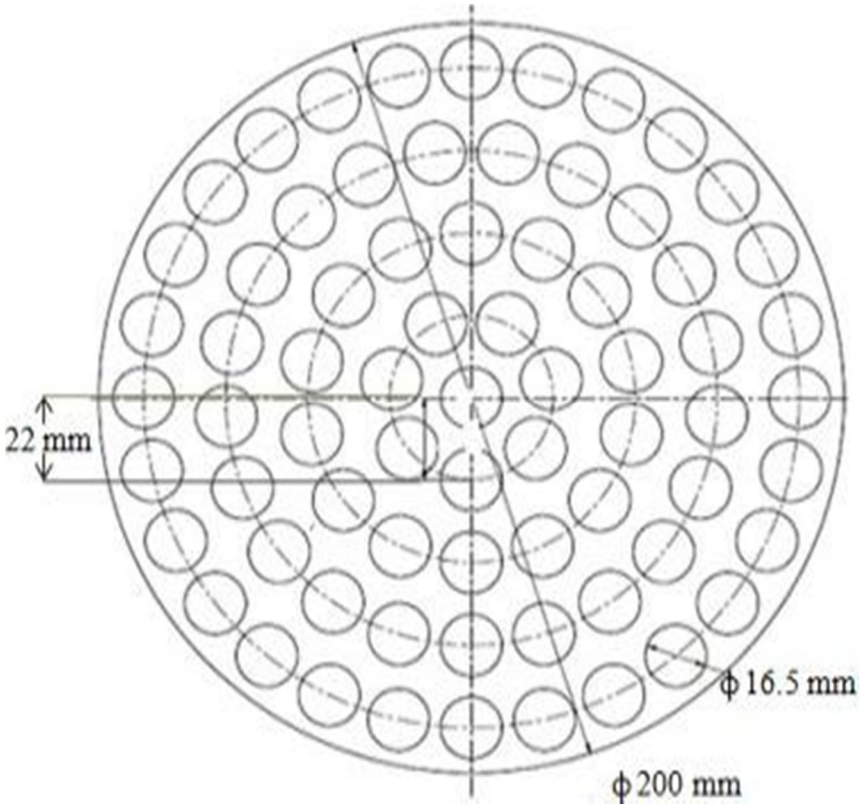

Fig. 3.1: Wire cutting Scheme.

D. Specimen Geometry

Cyclic stress response and fatigue life exhibited by a material are sensitive to the specimen geometry adopted for testing and hence stringent restrictions are imposed on the specimen design. In order to avoid anticipated failure at specimen's threads specimens with Hourglass and 6mm gauge diameter (D) were used in the present study as shown in (Fig. 3.2).

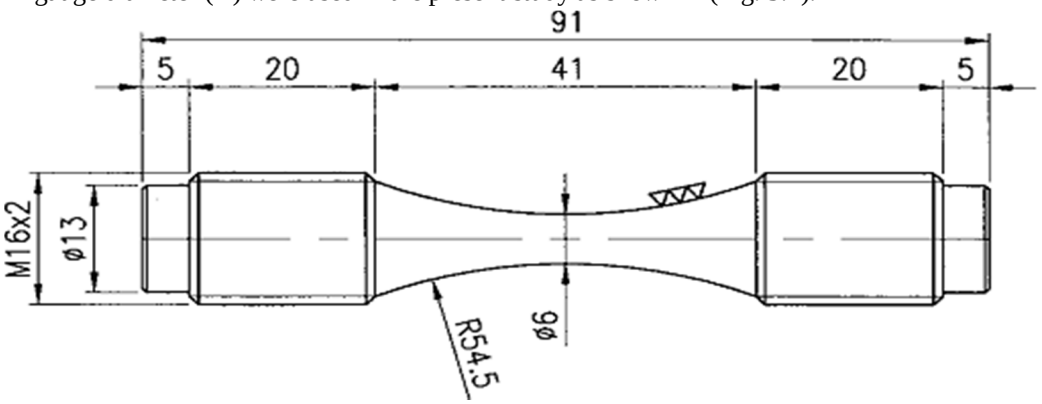

Fig. 3.2: Geometry of 10wt%Cr Steel specimen.

For HCF tests, solid cylindrical specimens with 25mm gauge length (L) and 10 mm gauge diameter (D) were chosen for the DMW as per ASTM (E 466-07) [19] shown in Fig. (3.3).

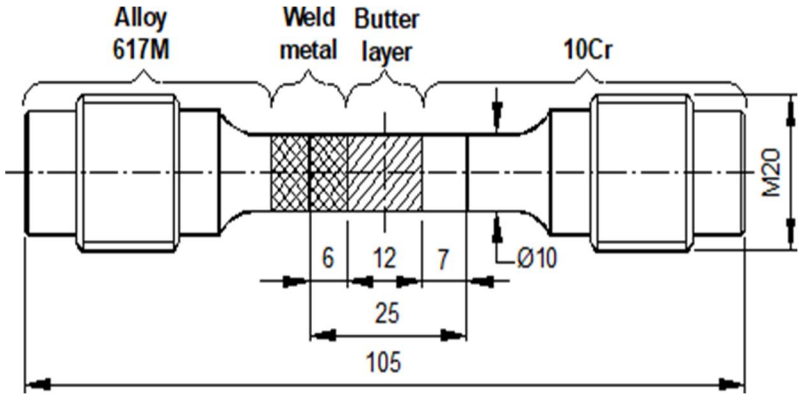

Fig. 3.3: Geometry of DMW specimen.

E. High Cycle Fatigue Test Procedure

The specimens were exposed to HCF cycling on an Electromagnetic resonance high cycle fatigue machine (Make: RUMUL) from 300 K-853 K employing different loading conditions. The specimen was mounted between the two adapters. For high temperature testing, specimens were subsequently heated in the resistance heating split type furnace. The heating of HCF samples was performed under zero load conditions and a thermocouple was attached to monitor the temperature. The machine has a maximum load capacity of $\pm$50kN, maximum

Stroke of 600 mm, minimum stroke of 320 mm, frequency range 40-220 HZ, R = -1 to +1,

Temperature range of 298 K to 1173 K. Continuous cycling HCF tests were conducted by employing a sinusoidal waveform of constant amplitude.

F. Working Principle of Resonance fatigue testing Machine

A cyclic load is produced in the specimen by exciting the natural resonance of a mass supported by a spring [20]. The specimen is the spring and the mass is incorporated in the machine structure. Resonance is maintained by an excited electromagnet, which only has to supply sufficient power to overcome the system damping losses. Mean load (either tensile or compressive) can be applied, by springs having much higher deflection per unit force than the specimen and they will have an insignificant effect on resonant properties of the specimen/mass system as illustrated in Fig. 3.4.

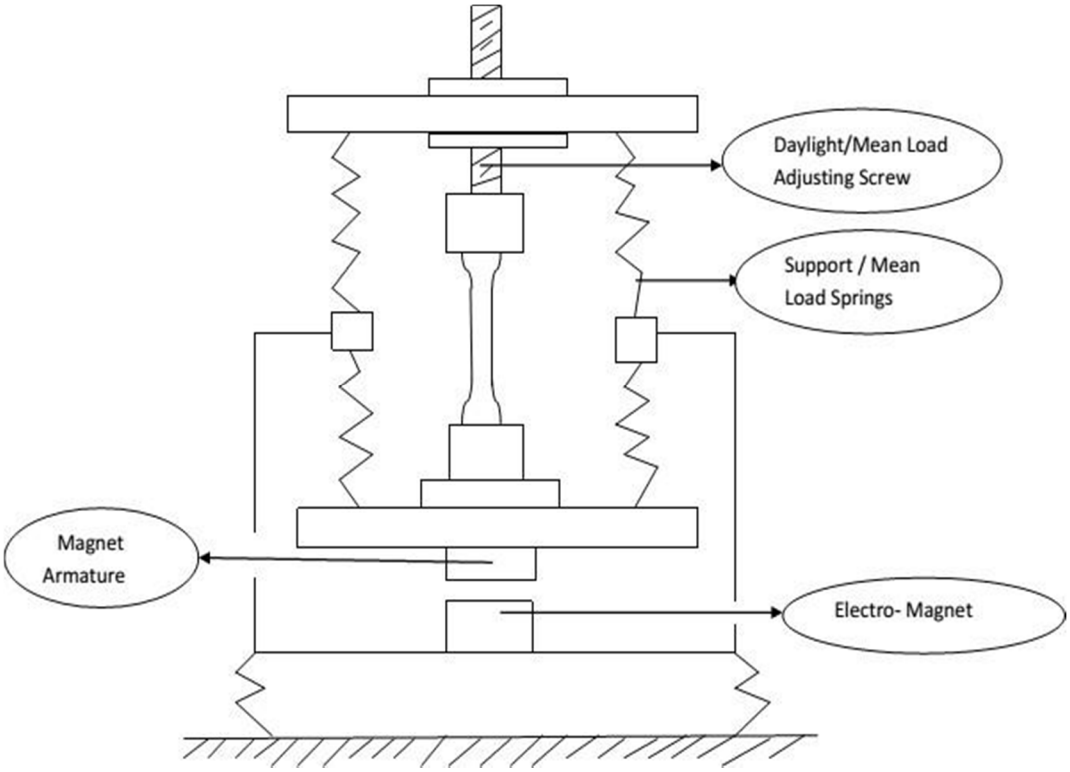

Fig. 3.4: Mechanical scheme of Electromagnetic Resonance (EMR) machine [20].

The armature of the electromagnet is rotated 180° in clock wise direction and remaining 180° in counter clockwise direction by a servo motor. In the electromagnetic field, the armature works as south and North Pole respectively, thus repelling or attracting the electromagnet with a frequency that is equal to the natural frequency of the attached spring/mass system which oscillates with a specific frequency. The specimen attached between the upper and the lower masses thus oscillates with that frequency, producing cyclic loading.

G. Test Matrix for HCF test

The materials under this investigation, 10wt%Cr steel, DMW are tested for their high cycle fatigue properties. In the present study tests at various temperatures with different combinations of alternating stress, mean stress and *R* has been performed as shown in the Tables (3.3, 3.4, and 3.5).

Table 3.3: Test matrix of 10wt% Cr steel from (300 K-853 K) and *R* = -1 (*) indicates data points used for modelling.

Temperature, K	300 K	673 K	853 K
Alternating stress (σ_a), MPa	355	300	200
	400	310	220
	450	320	235
	460	330	250
	475	340	300
	500	355	355
	550*	-	240*
	600	-	270*
	-	-	330*

Table 3.4: Test matrix of 10wt% Cr steel with different mean stress combinations at 853 K

Temperature, K	Alternating stress (σ_a), MPa	*R*
853	180*	-1
	200	
	250	
	200**	
	230**	

Table 3.5: Test matrix of DMW with *R* = -1 at 853 K, * Run-out, **DDMW.

1) *Scanning Electron Microscopy / Energy Dispersive X-Ray Spectroscopy (SEM/EDS):* SEM allows an area of interest to be examined at extremely high magnifications. SEM produces images of high resolution and detailed depth of field unlike those attainable using normal optical microscopy. As examples, surface structures, general anomalies, and areas of contamination can be easily identified. At the same time, Energy Dispersive X-Ray Spectroscopy (EDS), sometimes referred to as EDAX or EDX, can be used to obtain semi- quantitative elemental results about very specific locations within the area of interest. Hardness evaluation The Vicker hardness test is conducted on the tested and untested DMW. During testing load of 300 gems are applied and the hardness was evaluated in direction perpendicular to the loading at the center of each region, indents were taken 0.2 mm apart. The four indentations were taken to estimate the average value of hardness of the tested and untested DMW. The test matrix for Vicker hardness test is shown in Table 3.6.

Table 3.6: Test matrix for Hardness test of DMW.

Test condition	Alternating stress (MPa)	Temperature, K	*R*
Tested	180	853	-1
Untested	-	-	-

IV. RESULTS AND DISCUSSION

A. *Generation of S-N plot for 10wt%Cr Steel at Different Temperature*

The stress-life (S-N) plots for alloy 10wt%Cr steel at different temperatures ranging from 300 K-853 K are shown in Figs.4.1 (a-c). The test data is also shown in Table 4.1. The plots show typical S-N behavior, with a gradual increase in cyclic life with decrease in stress amplitude. The specimens which have not failed up to 10^7 cycles are indicated as *run-out*. The corresponding stress amplitude is taken as the endurance limit or fatigue limit of the material at that temperature. Run-out is indicated by an arrow in the Figs. (4.1 a-c).

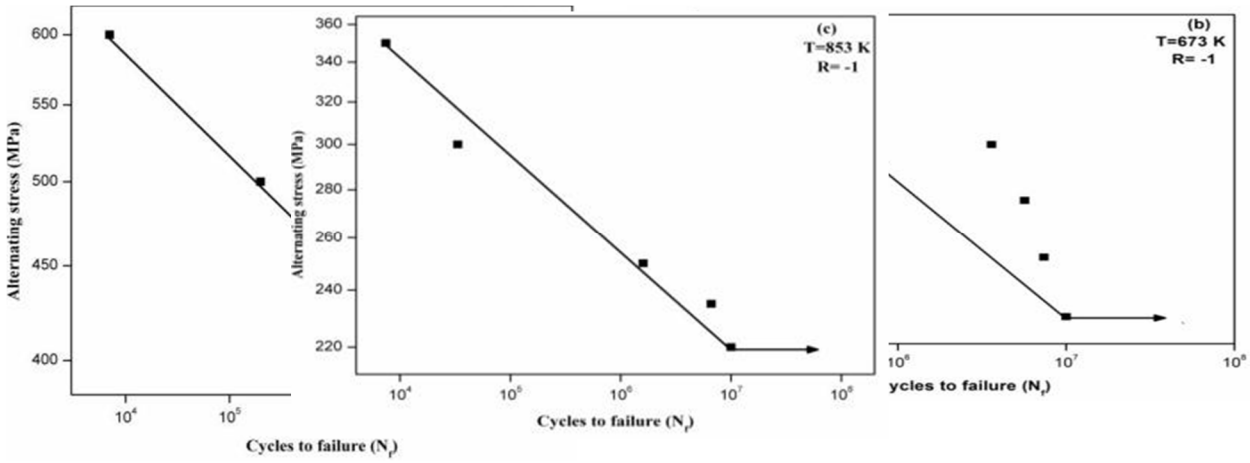

Fig. 4.1 (a-c): S-N plot of 10Wt%Cr Steel (a) at 300 K (b) at 673 K (c) at 853 K.

The plots show considerable scatter, especially at higher temperatures in comparison to room temperature (Figs. 4.1 a-c). This suggests that deformation mechanisms may be different at higher temperatures where the applied stress alone may not be the sole responsible factor in dictating fatigue life.

Temperature, K	300 K	673 K	853 K
Alternating stress (σ_a), MPa	355	300	200
	400	310	220
	450	320	235
	460	330	250
	475	340	300
	500	355	355
	550*	-	240*
	600	-	270*
	-	-	330*

Table 4.1: HCF test data at different temperatures. (*) indicates data points used for modelling

B. Comparative S-N plot for 10wt%Cr Steel at Different Temperatures

Fig. 4.2 shows the comparative S-N behavior at all temperatures. The plot shows that fatigue life is lower as the temperature is increased, irrespective of stress. This also leads to a lower value of the endurance limit as the temperature is increased (Table 4.2). It is also evident from Table 4.2 that there is a sharp decrease in endurance limit (as % of YS) from 51% to 46% when the temperature is increased from 300 to 673 K. However, the endurance limit remains more or less similar (45% of YS) when the temperature is further increased to 853 K, indicating strong temperature sensitivity of HCF behavior.

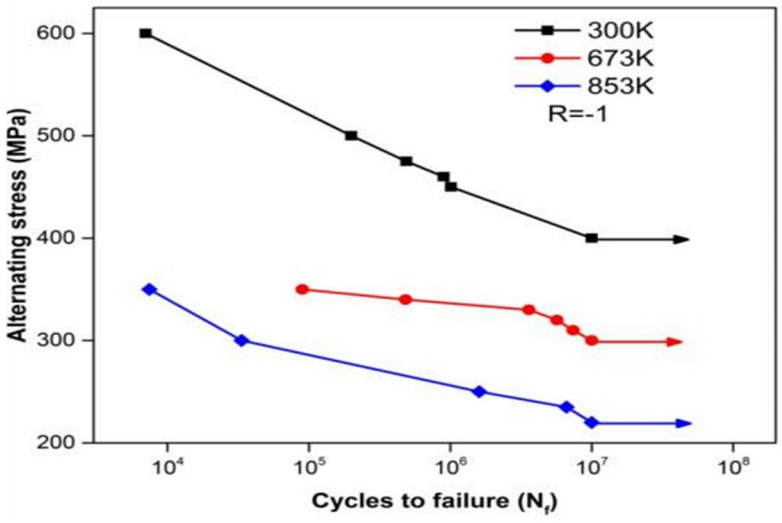

Fig. 4.2: Stress-life plot for 10wt%Cr Steel at different temperatures.

Table 4.2: Endurance limit stress (ELS) as % of YS and % of UTS 10wt%Cr steel

T (K)	YS(MPa)	UTS(MPa)	Endurance limit (MPa)	Endurance limit (% of YS)	Endurance limit (% of UTS)
300	783	899	400	51	44
673	641	714	300	46	42
853	483	500	220	45	44

C. It is observed from Fig.4.4 and Table 4.4 that there is a reasonable agreement between predicted and experimental life within scatter band 2.

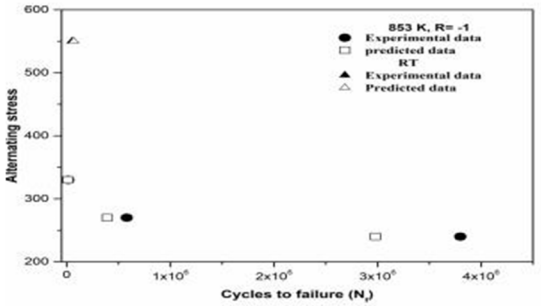

Fig.4.4: Comparison of predicted and experimental life using Fatigue parameters at 853 K and 300 K.

Temperature, K	Alternating stress (σ_a), MPa	Experimental life	Predicted life	Scater-band factor
853	240	3799657	2980135	1.27
	270	579785	392340	1.47
	330	15000	12400	1.20
300	550	52219	68035	1.30

Table 4.5: HCF test data at different stress ratios (R) at 853 K.

Mean stress (σ_m),MPa	Alternating stress (σ_a),MPa	R	Fatigue life, N_f
0	220	-1	10^7
50	200	-0.6	52,17571
55	190	-0.55	10^7
60	180	-0.5	10^7
80	160	-0.3	10^7
150	150	0	10^7
250	120	+0.35	10^7
300	90	+0.54	10^7
120	120	0	10^7
100	190	-0.31	10^7
170	170	0	10^7
70	220	-0.52	12,52018
210	210	0	3,34440
0	235	-1	66,26572
250	150	+0.25	10^7

D. Generation of Constant life Diagram (10^7) at 853 K

(σ_a) is plotted against (σ_m) at a given constant life (10^7) to obtain Goodman diagram. It demarcates safe and unsafe region, hence important design criterion. It is clearly seen from Fig.4.5 that the allowable stress decreases with increase in σ_m. HCF test data is also given in Table 4.5 with different values of *R*.

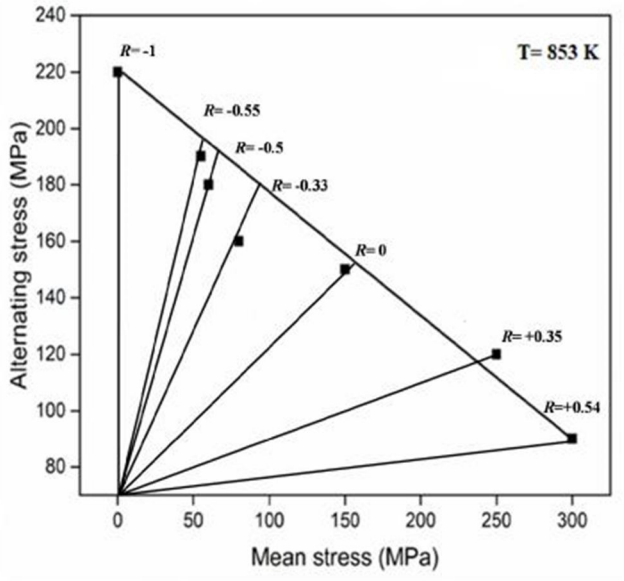

Fig. 4.5: Generation of constant life diagram (10^7) of 10wt%Cr at 853 K.

E. Generation of Haigh diagram at 853K

Goodman diagram is further extended in the form of Haigh in Fig.4.7. Haigh diagram is constructed by joining data points corresponding to approximately same life through different contours which also intersect different *R*-ratio. The numbers indicated adjacent to the life contours are the minimum lives corresponding to particular domain. Fig. 4.7 present the plot between the mean stress (σ_m) and alternating stress (σ_a) for a constant life. It may be noted here that for a given constant life contour, the stress amplitude required for a given value of mean stress is termed as "allowable stress"..

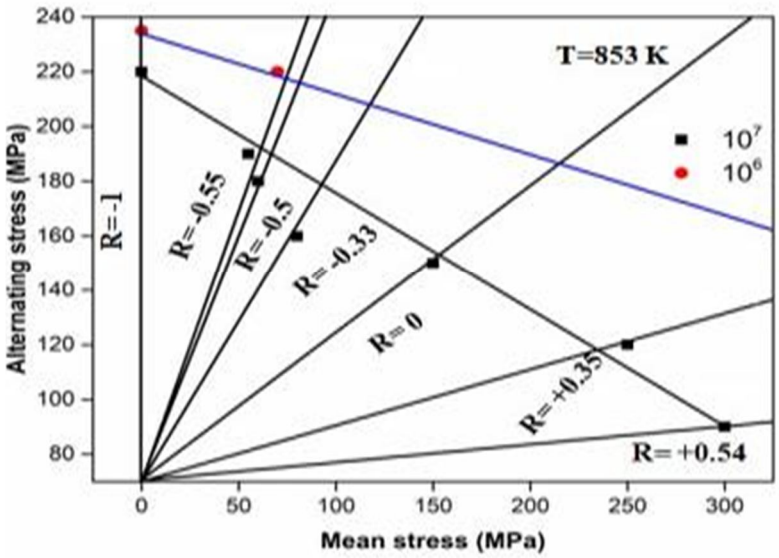

Fig. 4.7: Haigh diagram for alloy 10wt%Cr steel at 853 K.

F. Characterization studies

1) Replica: In-order to analyses the surface damage replica is taken. Replica is taken by applying acetate cartridge on the tested sample with the help of dispensing gun, before cutting the sample for optical and SEM analysis. It is clearly visible from Fig. 4.8 that there is no distinct slip activities apart from primary crack which is the typical characteristic of HCF.

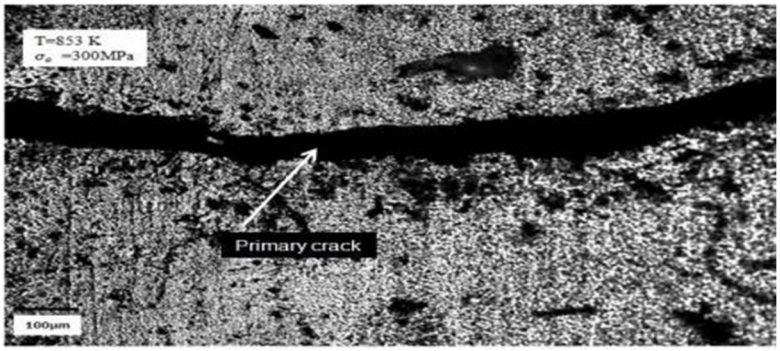

Fig.4.8: Replica image indicating the surface damage of 10wt%Cr Steel at 853 K, σ_a = 300 MPa, *R*= -1.

2) Initial Microstructure

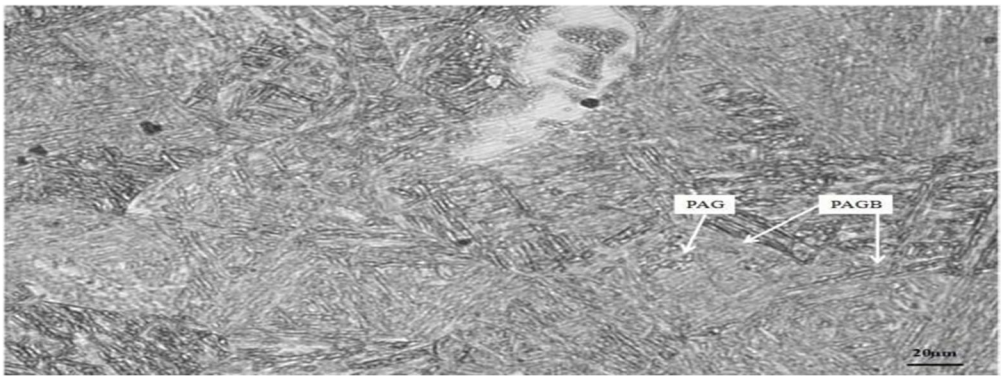

Fig. 4.9: Initial microstructure of 10wt%Cr Steel.

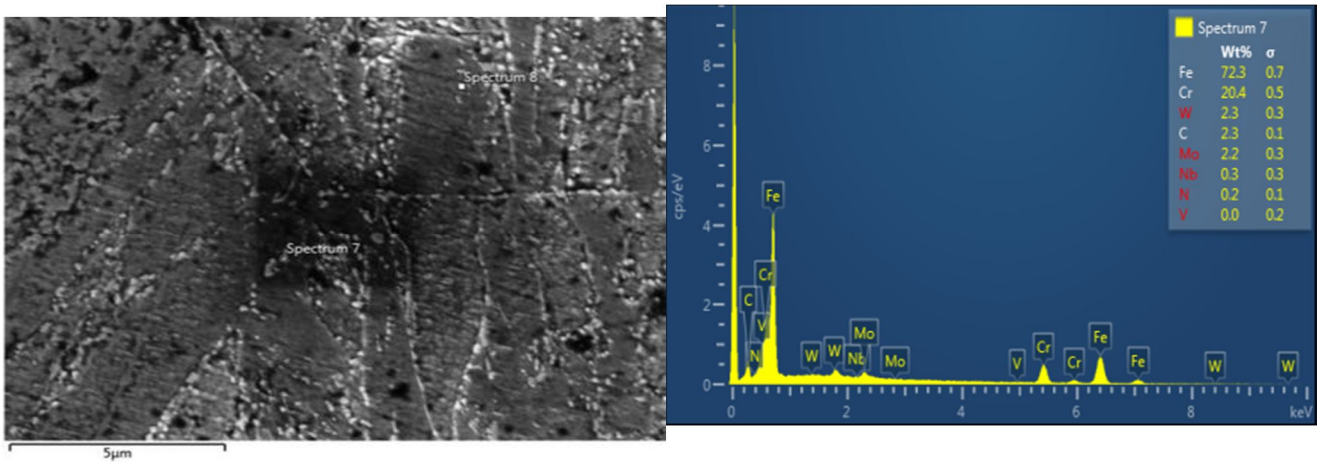

Fig.4.10 (a): SEM image of untested 10wt%CrSteel. Fig.4.10(b): EDS showing precipitates in untested 10wt%Cr Steel.

Figs. 4.9, 4.10 (a, b) shows the optical, SEM and EDS of 10wt%Cr Steel after normalizing and tempering treatment. Fig. 4.9 shows that prior austenite grains were of nearly 30μm average size and having tempered martensite structure with fine laths. It is clearly depicted from Fig. 4.10(a) that the prior austenite boundaries are decorated with the precipitates. The precipitates are Cr rich which is clearly indicated in Fig. 4.10(b).

3) *Fractography Studies:* Fracture surface images at different temperatures and stress amplitudes via 300 K (450 MPa), 673 K (340 MPa) are shown in Fig. 4.11(a and b) respectively. SEM fractograph showing masking of striations by oxide scales, of HCF tested 10wt%Cr steel at 853 K, σ_a = 355 MPa, R= -1 is shown in Fig.4.11(d). In Figs. 4.11(e and f) SEM Fractography showing strong oxidation of HCF tested 10 wt%Cr steel at 853 K, σ_a= 355 MPa, σ_m= 50 MPa.

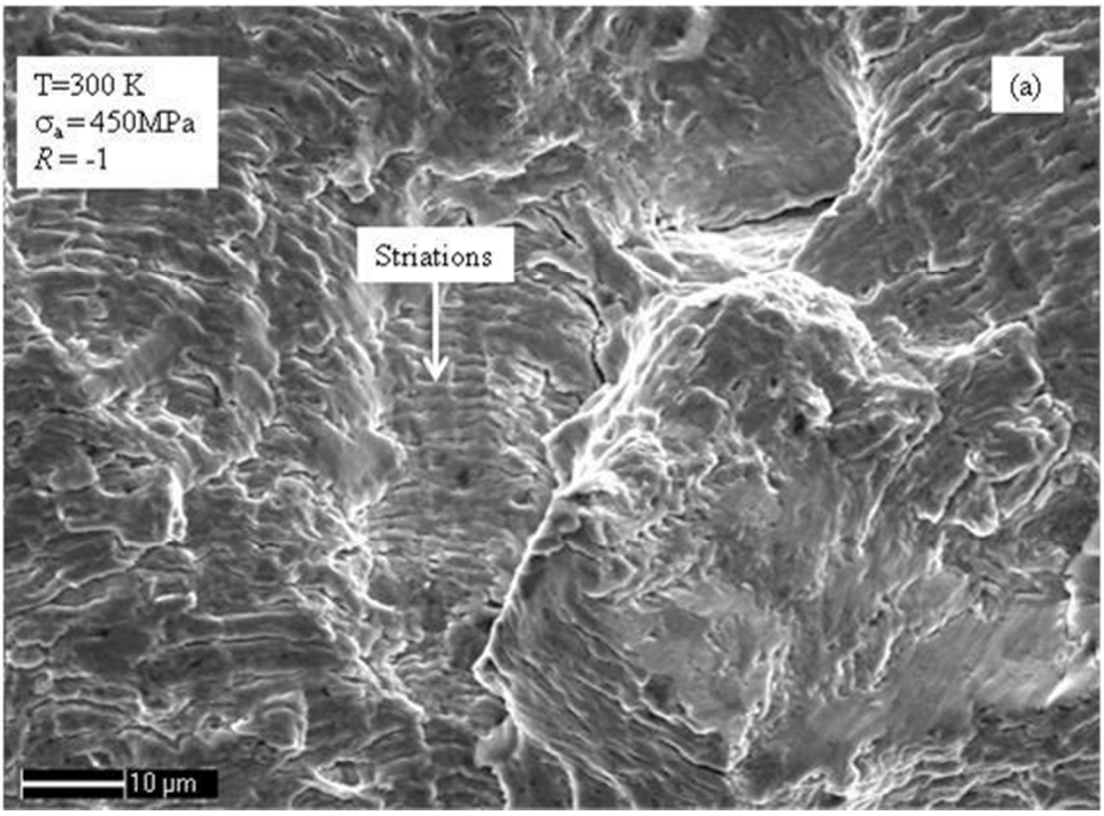

Fig. 4.11 (a) SEM fractograph showing striations at 300 K, σ_a= 450 MPa, *R*= -1.

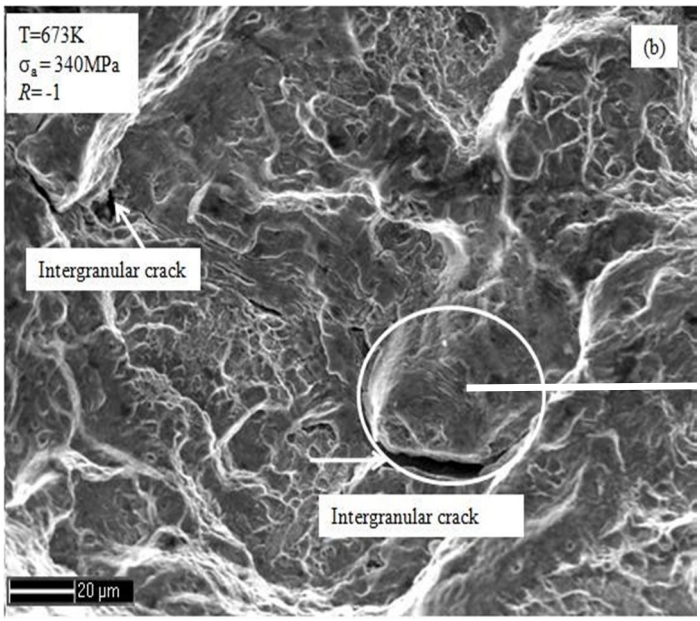

Fig. 4.11(b) SEM fractogragh showing mixed mode of failure at 673 K, σ_a= 340 MPa, *R*=- 1.

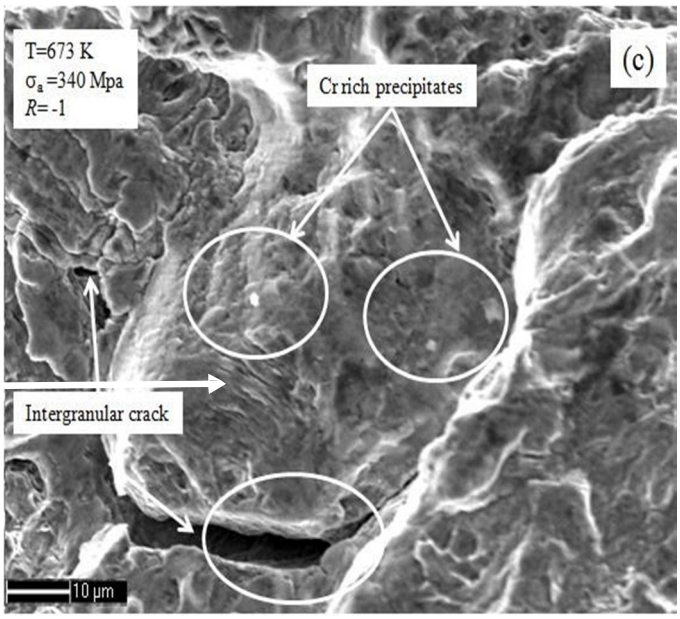

Fig. 4.11(c). SEM fractograph showing magnified view of Fig. 4.11 (b).

ISSN: 2321-9653; IC Value: 45.98; SJ Impact Factor: 7.429
Volume 9 Issue VI Jun 2021- Available at www.ijraset.com

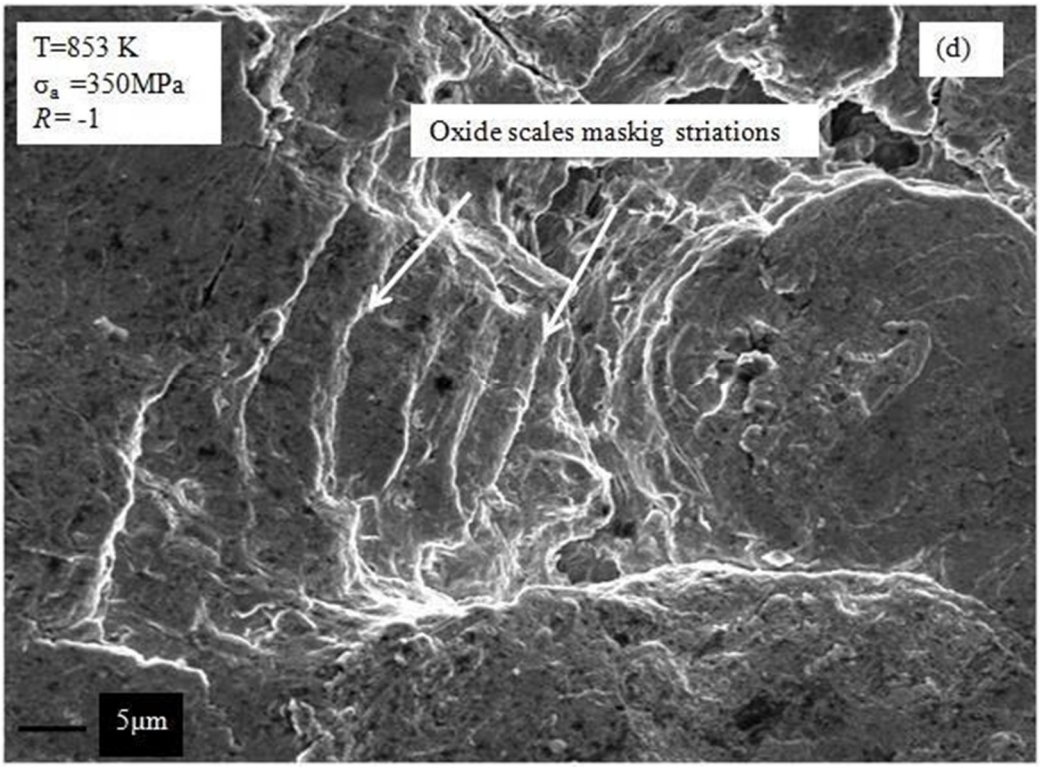

Fig. 4.11(d) SEM fractogragh showing oxide scales masking striations at 853 K, σ_a=355MPa, *R*= -1.

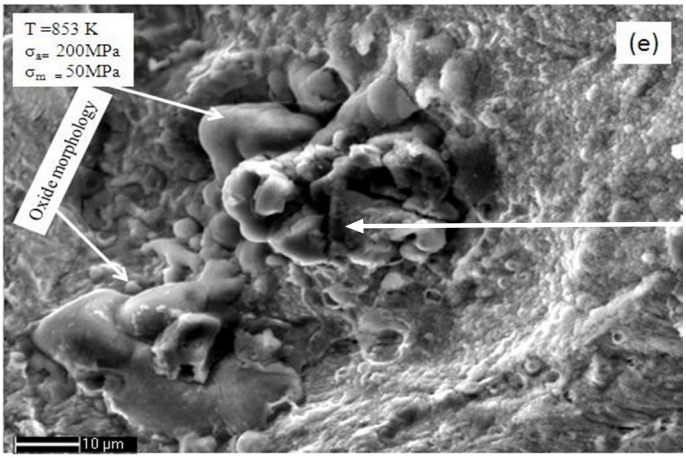

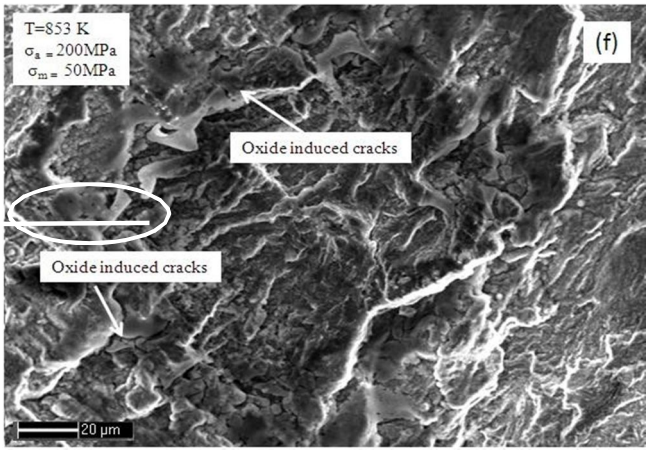

Fig. 4.11(e): SEM fractograph showing magnified view of Fig. 4.11(f). Fig. 4.11(f): SEM fractograph showing strong oxidation at 853 K, σ_a= 200 MPa, σ_m= 50 MPa.

Fig. 4.11 (a) shows trans-granular fatigue crack morphology marked by striations of the HCF tested specimen (300 K, σ_a=450 MPa, R=-1). Fig. 4.11 (b) shows mixed mode crack propagation behavior which is manifested from the inter-granular cracks (marked in the Fig. 4.11(b)) apart from striations of the HCF tested specimen (673 K, σ_a=450 MPa, R=-1) selected portion of Fig. 4.11 (b) is magnified in the Fig. 4.11(c) which shows the inter-granular crack in a greater detail. Cr rich precipitates are also observed. Effect of oxidation is also clearly reflected from the oxide scales. Similar effect is also shown in Fig. 4.11(d) HCF tested (853 K, σ_a=355 MPa, R= -1). Fig. 4.11(e and f) shows the effect of mean stress and it is clearly observed that there is a strong oxidation effect as the distinct oxidation morphology is formed on the fracture surface. Oxide is generally brittle in nature and during fatigue testing the brittle oxide will not undergo deformation, this eventually leads to breakage of oxide scales leading to formation of oxide induced cracks.

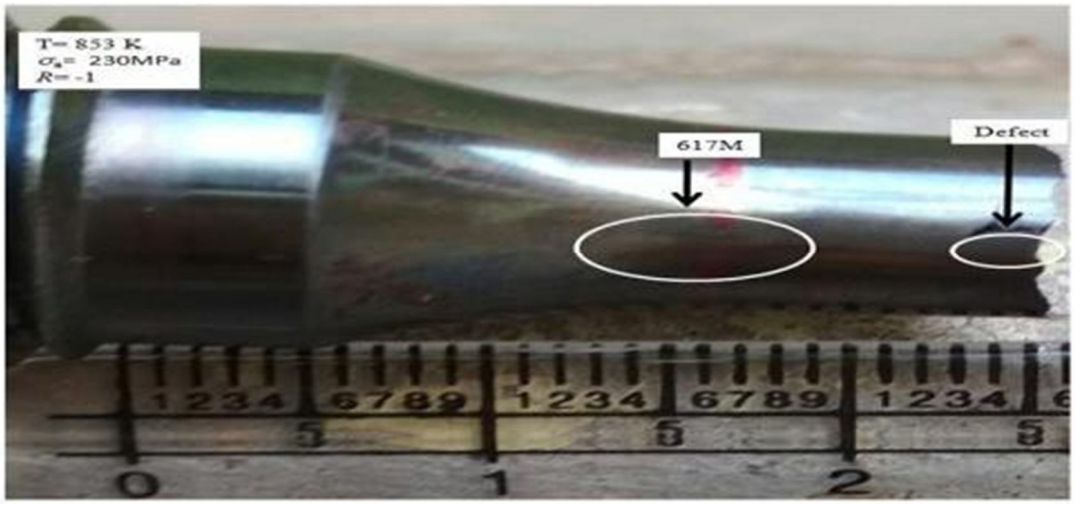

Fig.4.13: Failure location of DDMW HCF tested sample at 853 K, σ_a = 230 MPa, *R*= -1.

It is clear from SEM images that apart from applied stress, oxidation has also an important role in fatigue life particularly at higher temperature.

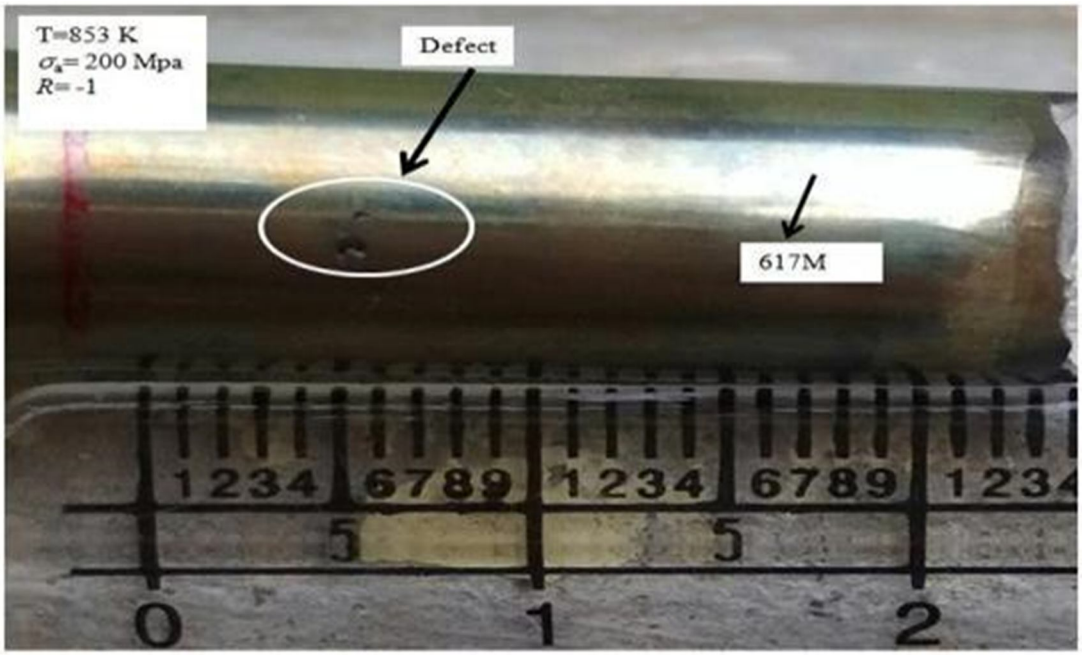

Fig. 4.14: Failure location of DDMW HCF tested sample at 853 K, σ_a = 200 MPa, *R*= -1.

G. Vicker Hardness Test

Vicker hardness test has been conducted on the tested and untested specimen. It is clearly shown in the Fig. 4.15 (black dot represents tested specimen, red dot represents untested specimen) that the hardness of the tested specimen (853 K, σ_a=180MPa, *R*=-1), increases in the butter layer but decreases in the 10wt%Cr side compared to untested. The significant increase in the hardness value in butter layer could be attributed to In-situ □' precipitate at 853 K on the tested specimen, on the other hand the decrease in the hardness value in the tested specimen is due to possible softening of Cr rich precipitates. However, it may be noted that increase in the hardness in the tested compared to untested far exceeds that of the decrease in the hardness of 10wt%Cr side. The reason for this could be that coarsening of the Cr-rich carbide precipitates generally required a longer time which may not be available in the shorter duration of HCF test. On the other hand, temperature of 853 K

ISSN: 2321-9653; IC Value: 45.98; SJ Impact Factor: 7.429
Volume 9 Issue VI Jun 2021- Available at www.ijraset.com

V. CONCLUSIONS AND FUTURE SCOPE OF THE WORK

The present work deals with the elevated temperature high cycle fatigue characterization of 10wt%Cr Steel and DMW a candidate material for rotor of Indian advanced ultra-supercritical (A-USC) program. Major conclusions derived from the investigation are summarized as follows:

A. *Conclusions*

1) Increase in temperature results in decrease in fatigue life of 10wt%Cr Steel irrespective of the stress amplitude.
2) As temperature is increased from 300 K-673 K, there is a sharp decrease in endurance limit (as % of YS) from 51% - 46% while it remains more or less similar (45% of YS) when temperature is further increased to 853 K.
3) Fatigue parameters derived from Basquin equation show that with increase in temperature fatigue strength coefficient decreases.
4) The combined effect of mean stress and alternating stress with different combinations of R value is presented in the Haigh diagram, giving clearly safe and unsafe zone.
5) It is clarified from the SEM images that apart from striations, inter-granular cracks, and oxide-induced cracks are also responsible for the fatigue failure at high temperature.
6) Hardness value of tested DMW decreases in the 10wt%Cr side, while it increases in the butter layer side as compared to untested DMW.

B. *Future Scope of Work*

1) In the present work, Haigh diagram is developed for two constant lives at 853 K, Haigh diagram can be extended for other constant lives.
2) Precipitation of carbides is very effective during fatigue deformation at elevated temperatures. It is important to characterize the type and morphology of these precipitates and their implication on the HCF life.
3) Effect of mean stress on fatigue life of DMW can be developed.
4) Detailed scanning electron microscopy is need to be developed for the DMW.
5) Microstructure of different zones of DMW can also be analyzed.

VI. ACKNOWLEDGEMENT

I express my sincere gratitude to the Desh Bhagat University Mandi Gobindgarh for giving me the opportunity to work on the thesis during my final year of M.Tech. In Mechanical Engineering.
I would like to thank my supervisor Er. Puneet Bansal, Assistant Professor of Department of Mechanical Engineering at Desh Bhagat University Mandi Gobindgarh for his kind support and healthy criticism throughout my thesis which helped me immensely to complete my work successfully.
I also owe my sincerest gratitude towards Head of Department of Mechanical Engineering at Desh Bhagat University Mandi Gobindgarh for his valuable advice.
Last but not least, a word of thanks for the authors of all those books and papers which I have consulted during my dissertation work as for preparing this report.

REFERENCES

[1] N. C. Bhatt, Maneesh Batrani, Jatinder Mohan, V. Gopalakrishnan & M. K. Verma, “Indian AUSC Steam Turbine Program – Current Status and Future Program,” International Journal of Engineering Research & Technology (IJERT), 2015, v. 4, pp. 291-293.
[2] Sc chetal, T jayakumar & Ak bhaduri, “Material Research and Opportunities in Thermal (coal based) power sector including Advanced Ultra Super Critical Power Plants,” Proc Indian Natn Sci Acad, 2015, 81, pp. 739-754.
[3] R. Blum, R.W.Vanstone, “Materials development for boilers and steam turbines operating at 700°C,” In Proceedings of the 6th International Charles Parsons Turbine Conference. Dublin, Ireland, 2003, pp. 498-510.
[4] K. Metzger, K. H. Czychon, K. Maile, A. Klenk, A. Helmrich, Q. Chen.GKM test rig: “Investigation of the long term operation behavior of tubes and forgings made of alloys for future high efficient power plants,” Advances in Materials Technology for Fossil Power Plants: Proceedings from the Sixth International Conference, Materials Park, OH: ASM International, 2013, pp. 86–95.
[5] A. Di Gianfrancesco, A. Tizzanini, M. Jedamzik, C. Stolzenberger, “ ENCIO project: An European approach to 700 °C power plant,” Advances in Materials Technology for Fossil Power Plants: Proceedings from the Seventh International Conference.
[6] Materials Park, OH:ASM International, 2013, pp. 9–23
[7] M. Fukuda, et al. “Advanced USC technology development in Japan,” Advances in Materials Technology for FossilPower Plants: Proceedings from the Seventh International Conference. Materials Park, OH: ASM International, 2013, pp. 24–40.

[8] A. Mathur, O. P. Bhutani, T. Jayakumar, D. K. Dubey, S. C. Chetal. India's national A-USC mission—Plan and progress. Advances in Materials Technology for Fossil Power Plants: Proceedings from the Seventh International Conference. Materials Park, OH: ASM International, 2013, pp. 53–59.
[9] Ghazwan M Al Qaraghuli, "High cycle fatigue testing of Steel for Federal Aviation administration (FAA) part qualification," California state university, Sacramento, 2017.
[10] R.W. Hertzberg, "Deformation and Fracture mechanics of engineering materials," John Wiley &Sons, Inc., ISBN: 0-471-01214-9.
[11] Elements of metallurgy and engineering alloys, chapter 14, ASM international (2008).
[12] George E. Dieter, "Mechanical Metallurgy," 3rd edition, McGraw-Hill education publications.
[13] R. L. Klueh "Elevated-temperature ferritic and martensitic steels and their application to future nuclear reactors," U.S. department of energy, 2004.
[14] D. R. Amos, Charlotte, NCR. D. Conroy, Newcastle upon Tyne, UK, retired W. Janssen and T.-U. Kern, Muelheim, Germany, "Advanced fabricated 10Cr rotor technology for increased efficiency," 2006, pp. 1-8.
[15] W. C. Leslie, Met. Trans. 3, 1972, pp. 5-17.
[16] J. Nutting, "Advanced Heat Resistant Steel for Power Generation," The Institute of Materials, London, 1999, pp. 12-30.
[17] J. Pasupathy, V. Ravisakar, " Detailed study on Disimilar Welding of Low Carbon Steel with AA 1050 using TIG Welding," International journal of Engineering Research and Technology, 2013, v. 2, pp. 1588-1594.
[18] A. Sarkar, A. Nagesha, R. Sandhya, K. Laha, A.K. Bhaduri "Influence of dynamic strain aging on high cycle fatigue behavior of alloy 617M," Trans Indian Inst. Met. 69 (2) (2016) 399-402.
[19] W. Chen, M.C. Chaturvedi, "On the mechanism of serrated deformation in aged Inconel 718," Material science and engineering A229 (1997), 163-168.
[20] C. Cabet, L. Carrol, R. Wright "Low cycle fatigue and creep-fatigue behavior of alloy 617 at high temperature," Journal of pressure vessel technology, Dec 2013, v. 135,
[21] Standard practice for conducting force controlled constant amplitude axial fatigue tests of metallic materials, ASTM, E 466-07.
[22] Sanjay Chauhan, Revival of an Electro-Magnetic Resonance (EMR) Machine, Department of Mechanical Engineering, NIT Rourkela (2010).

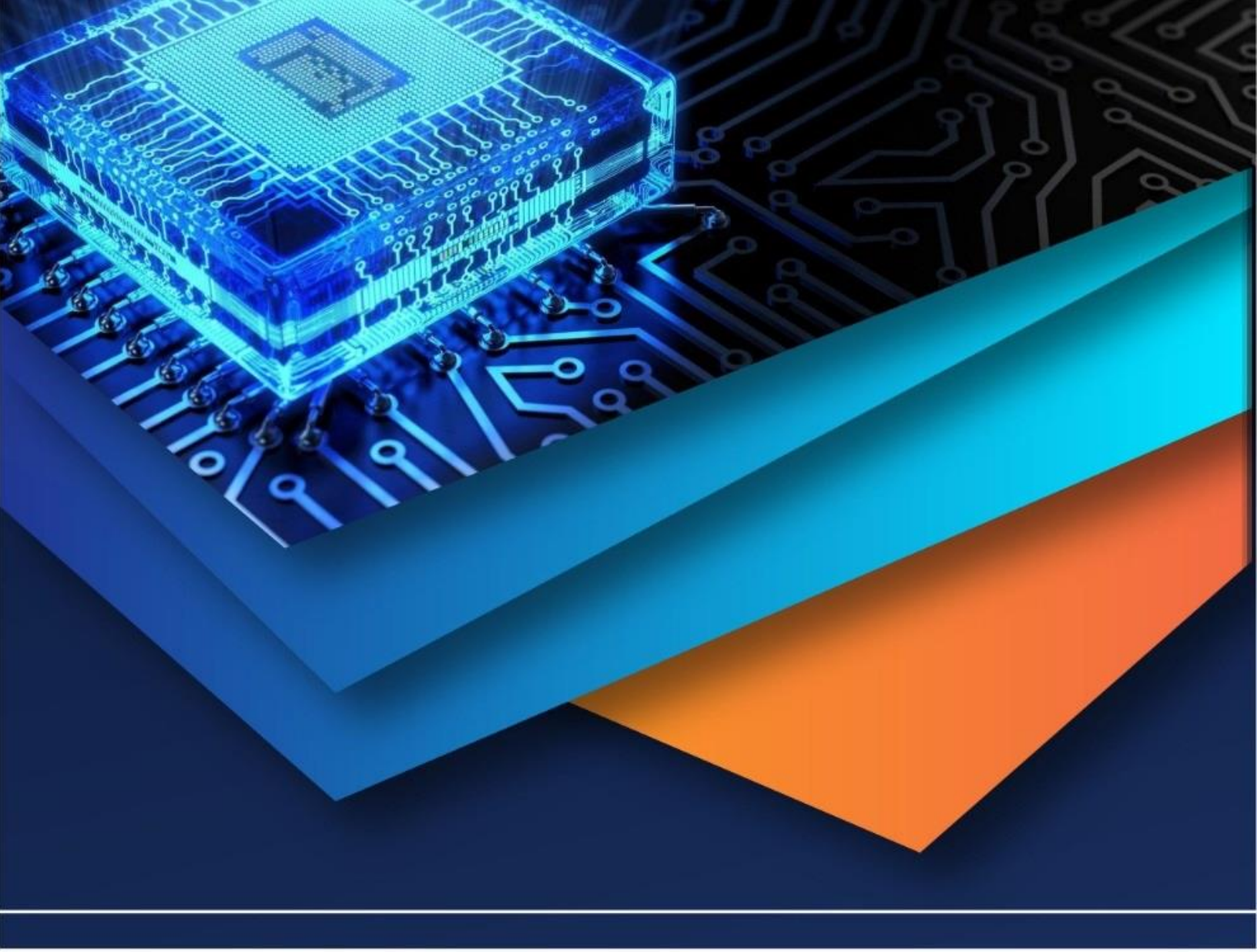

10.22214/IJRASET

45.98

IMPACT FACTOR: 7.129

IMPACT FACTOR: 7.429

INTERNATIONAL JOURNAL FOR RESEARCH

IN APPLIED SCIENCE & ENGINEERING TECHNOLOGY